Accesses to electronic structures and the excited states of iridium complexes containing pyrazolyl or benzimidazoly ligands: A DFT/TDDFT exploitation

ARTICLE *in* INORGANICA CHIMICA ACTA · MAY 2014

Impact Factor: 2.05 · DOI: 10.1016/j.ica.2014.03.031

6 AUTHORS, INCLUDING:

Feng Zhao
Jiangxi Science & Technology Normal Univ…
51 PUBLICATIONS **189** CITATIONS

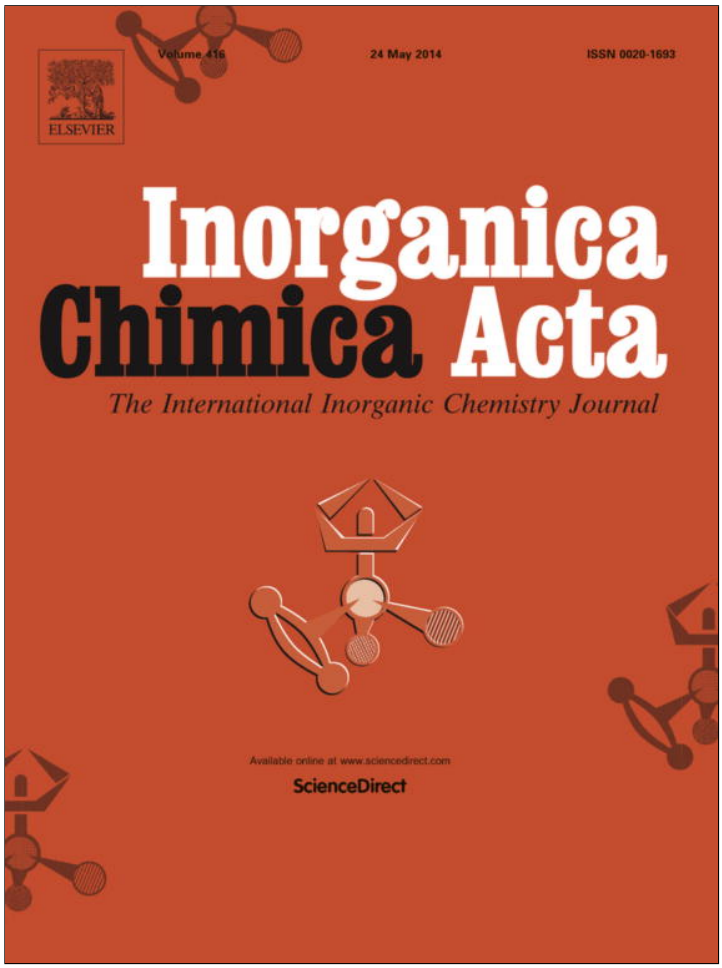

Inorganica Chimica Acta 416 (2014) 180–185

Contents lists available at ScienceDirect

Inorganica Chimica Acta

journal homepage: www.elsevier.com/locate/ica

Accesses to electronic structures and the excited states of iridium complexes containing pyrazolyl or benzimidazoly ligands: A DFT/TDDFT exploitation

Qiang Li [a], Zhenhua Xiong [b], Hongying Xia [b], Feng Zhao [a,*], Wenqu Liu [a], Yibo Wang [c]

[a] Jiangxi Key Laboratory of Organic Chemistry, Jiangxi Science and Technology Normal University, Fenglin Street, Nanchang, Jiangxi 330013, PR China
[b] School of Chemistry and Chemical Engineering, Jiangxi Science and Technology Normal University, Fenglin Street, Nanchang, Jiangxi 330013, PR China
[c] Key Laboratory of Guizhou High Performance Computational Chemistry, Department of Chemistry, Guizhou University, Guiyang 550025, PR China

ARTICLE INFO

Article history:
Received 23 November 2013
Received in revised form 12 February 2014
Accepted 23 March 2014
Available online 1 April 2014

Keywords:
Iridium complex
Density functional theory
Metal-centered state
Deactivation pathway
Lack of emission

ABSTRACT

The ground state, ^{3}MLCT and ^{3}MC excited states of two Ir complexes Ir(dfbpzb)(ppy)Cl (**1**) and Ir(Mebib)(ppy)Cl (**2**) where dfbpzb = 1,5-difluore-2,4-bis(3-methylpyrazolyl)benzene, ppy = 2-phenylpyridine, and Mebib = bis(*N*-methylbenzimidazoly)benzene, have been investigated using density functional theory (DFT) and time-dependent density functional theory (TDDFT). The substitution from dfbpzb ligand to Mebib ligand induces a significant change on the luminescent properties of complexes **1** and **2**. The complex **1** does not emit at room temperature, while complex **2** does. The UV–Vis absorption spectra of both complexes are well reproduced by TD-DFT calculations. Importantly, the triplet metal-to-ligand charge transfer (^{3}MLCT) and metal-centered (^{3}MC) states were discussed in detail by excited state calculations, and the ^{3}MLCT → ^{3}MC deactivation pathway was demonstrated as an important factor for the lack of emission for the investigated complex **1**.

1. Introduction

Transition metal complexes have attracted much attention because of the richness and variety of their photophysical properties [1–3]. A nearly 100% quantum yield of triplet emission may be achieved for transition metal complexes owing to the heavy atom induced spin orbit coupling effects, especially for Ru, Os, and Ir complexes [4–6]. Generally, the photophysical properties of these complexes are governed by the lowest lying triplet excited states, i.e. metal-to-ligand charge transfer (^{3}MLCT) [7]. Additionally, ligand-to-ligand charge transfer (^{3}LLCT) and intraligand charge transfer (^{3}ILCT) states may be involved [8,9], only depending on the order of energy levels of those states. In contrast, little is known about the metal-centered (^{3}MC) states of these complexes, which are the non-radiative states [10]. The energy gaps between the ^{3}MC states and optically-active ^{3}MLCT states strongly affect the emission properties of such complexes [11–13]. To control and regulate the photophysical properties of these metal complexes, it is necessary to understand fundamental information on the ^{3}MC states. Recently, temperature-dependent luminescent studies have been used to investigate the relationship between the ^{3}MLCT and ^{3}MC states [14]. However, since the ^{3}MC states are usually dark states that cannot be directly detected by experimental approaches [15], it is not still easy to understand how those states affect the luminescence properties of metal complexes.

Density functional theory (DFT) and time-dependent density functional theory (TDDFT) have shown powerful advantages for investigation of electronic structures of excited states of transition metal complexes [16–18]. In this paper, we focused on the theoretical studies of the excited states of two Ir complexes Ir(dfbpzb)(ppy)Cl (**1**) and Ir(Mebib)(ppy)Cl (**2**) using DFT and TDDFT, where dfbpzb = 1,5-difluore-2,4-bis(3-methylpyrazolyl)benzene, ppy = 2-phenylpyridine, and Mebib = bis(*N*-methylbenzimidazoly)benzene. Complex **1** is nonemissive in CH_2Cl_2 at room temperature, while complex **2** is highly emissive [19,20]. A thorough comparison of two complexes with the large difference in observed emission properties would give useful insights into the design of new photoactivable metal complexes with tunable photophysical features.

2. Computational method

The ground state geometry optimization of Ir(III) complex was carried out using the B3LYP exchange–correlation functional [21,22]. A double-ξ quality LANL2DZ basis set [23,24] was employed for the Ir atom and a 6-31G* type basis set [25,26] for

* Corresponding author. Tel.: +86 79183805183.
E-mail address: zhf19752003@163.com (F. Zhao).

http://dx.doi.org/10.1016/j.ica.2014.03.031
0020-1693/

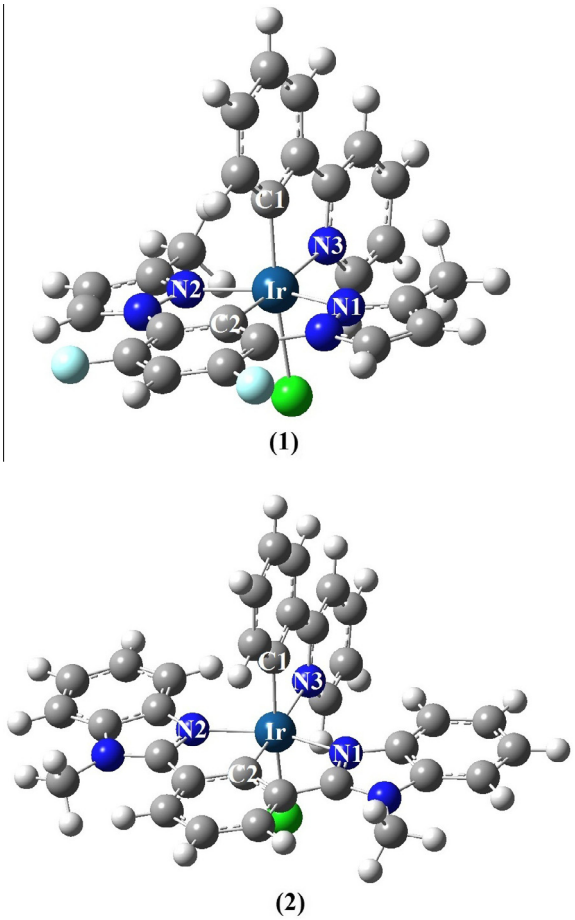

Fig. 1. Optimized ground state geometric structures of (**1**) Ir(dfbpzb)(ppy)Cl and (**2**) Ir(Mebib)(ppy)Cl.

C, H, N and Cl atoms. The geometries of the triplet excited states at the spin-unrestricted UB3LYP level with a spin multiplicity of **3**. The TDDFT calculations using the PBE1PBE functional [27,28] for the simulated UV–Vis absorption spectra of **1** and **2** were then performed based on the optimized geometries at ground state with the polarized continuum model (PCM) [29,30]. This functional has been proved to improve the accuracy of excitation energies in metal complexes [31,32].

Here, the B3LYP/6-31G*/LANL2DZ level of theory was employed to optimize the ground state geometry since it could give out satisfied geometry parameters (see below). However, a poor description of absorption properties of the involved complexes was encountered. Take complex **2** as example, the absorption maxima 428 nm calculated by the B3LYP functional is red-shifted about 24 nm as compared with the experimental 404 nm. On the other hand, the calculated absorption peak is at 407 nm with the PBE1PBE functional (only overestimated by 3 nm). Therefore, we have employed the PBE1PBE/6-31G*/LANL2DZ for further absorption spectra calculations.

Calculated electronic density plots for the frontier molecular orbitals and absorption spectra were prepared using GAUSS VIEW 4.1.2 software. In addition, the simulated absorption spectra were visualized with Gaussian bands-shapes with the value of 1200 cm^{-1} of the full-width at half-maximum (fwhm). All calculations were performed with the GAUSSIAN 09 software package [33].

3. Results and discussion

3.1. Ground state geometries and frontier molecular orbital

The optimized ground state geometries of the complexes **1** and **2** in the gas phase are presented in Fig. 1 and selected bond lengths and angles are summarized in Table 1. Vibrational frequencies were calculated using the optimized geometries to verify that those geometries represented a minimum on the potential energy surface. The geometry parameters of complex **2** are in general agreement with the experimental values of structural analogs Ir(Mebib)(mppy)Cl [19]. The calculated bond lengths of complex **2** are slightly overestimated by about 0.01–0.06 Å in comparison with the experimental values. The calculated bond angles deviate slightly (less than 4°) from the experimental values. The discrepancy should come from the crystal lattice distortion existing in the real molecules.

For complex **1**, HOMO and HOMO−1 are largely localized on the metal Ir atom and Cl atom. HOMO−2 mainly distributes over the Cl atom. However, LUMO and LUMO+2 are π^* orbitals localized on the ppy ligand, whereas LUMO+1 is a π^* orbitals localized on the dfbpzb ligand, with a few compositions from ppy ligand (Fig. 2, top). For complex **2**. HOMOs have orbital composition very similar to that for **1**. In contrast, LUMOs have different orbital compositions with respect to that of **1**. LUMO and LUMO+2 mainly reside on the Mebib ligand, whereas LUMO+1 is mainly localized on the ppy ligand. The substitution from dfbpzb ligand to Mebib ligand

Table 1
Main geometry structural parameters of **1** and **2** in the ground (S_0), the lowest triplet state (T_1), and the triplet metal-centered state (^{3}MC).

	1			**2**			Exptl[a]
	S_0	T_1	^{3}MC	S_0	T_1	^{3}MC	
Bond length(Å)							
Ir–N1	2.094	2.093	2.496	2.082	2.045	2.526	2.071
Ir–N2	2.094	2.093	2.494	2.082	2.043	2.526	2.041
Ir–N3	2.192	2.171	2.160	2.200	2.218	2.171	2.142
Ir–C1	2.033	1.997	2.027	2.030	2.031	2.029	2.001
Ir–C2	1.946	1.954	2.033	1.953	1.971	2.026	1.922
Ir–Cl	2.526	2.513	2.443	2.524	2.486	2.446	2.487
Bond angle (°)							
N1–Ir–N2	157.6	157.7	147.5	158.0	159.8	148.3	157.7
N1–Ir–C1	92.5	92.3	88.9	92.2	91.0	88.1	92.8
C1–Ir–N3	78.6	80.6	79.2	78.6	78.7	79.0	79.9
C1–Ir–Cl	170.9	172.5	172.2	170.7	170.6	172.1	172.0
C2–Ir–Cl	91.3	89.7	89.9	91.3	91.6	90.0	94.5
C1–Ir–N2	92.4	92.3	89.1	92.2	91.0	88.3	89.8
C2–Ir–N3	176.5	178.5	177.1	176.6	176.5	176.9	173.3

[a] From Ref. [19].

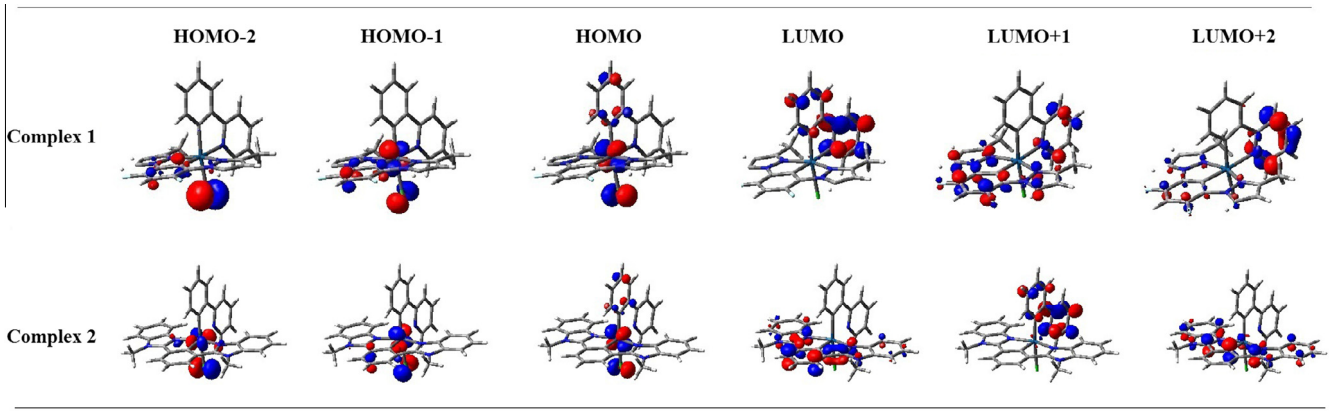

Fig. 2. Frontier molecular orbitals (isovalue = 0.06) of the complexes **1** and **2** calculated at the TDDFT (B3LYP)/6-31G*/LANL2DZ level at gas phase.

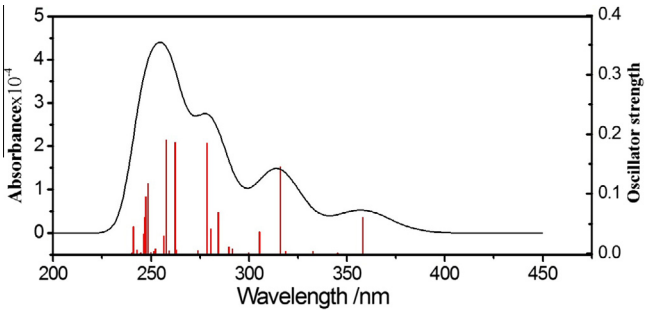

Fig. 3. Simulated absorption spectra in CH_2Cl_2 at the TDDFT (PBE1PBE)/6-31G*/LANL2DZ level for **1**. The excited states are shown as vertical bars with height equal to the oscillator strength values (red). (For interpretation of the references to color in this figure legend, the reader is referred to the web version of this article.)

results in a significant change on the electron density of the LUMOs, which is responsible for theirs photophysical properties.

3.2. Absorption spectra

The simulated absorption spectrum of complex **1** in CH_2Cl_2 solvent is reported in Fig. 3, and the detailed data including the calculated transitions in terms of energies, oscillator strengths, and compositions are presented in the Table 2. We computed absorption bands at 358 and 316 nm to be corresponding with experimental bands at 384 and 338 nm. The band at 358 nm was assigned as pure HOMO → LUMO transition with the spin-allowed metal-to-ligand charge transfer (^{1}MLCT)/ligand-to-ligand charge transfer (^{1}LLCT)/intraligand charge transfer (^{1}ILCT) characters. The band at 316 nm was mainly attributed to the transition of HOMO−1 → LUMO+1 with ^{1}MLCT/^{1}ILCT characters. In addition, it is worth noting that the band at 443 nm with spin-forbidden ^{3}ILCT/^{3}MLCT/^{3}LLCT character was calculated, which are corresponding to the very weak experimental absorption band at 411 nm.

The absorption spectrum of complex **2** was simulated and is reported in Fig. 4. The pure transition of HOMO → LUMO with ^{1}MLCT characters at 407 nm can be tentatively assigned to the experimental absorption band at 404 nm. The prominent band at 390, which is corresponding to the experimental absorption peak of 360 nm, was attributed to the main transition of HOMO−1 → LUMO with ^{1}MLCT/^{1}ILCT characters. The calculated absorption peak at 306 nm was dominated by the HOMO–4 → LUMO transition giving rise to ^{1}MLCT/^{1}LLCT/^{1}ILCT character, which is well in agreement with experimental UV–Vis peak at 299 nm. Additionally, the weak and long energy transition bands observed experimentally around at 523 and 472 nm may correspond to the theoretically spin-forbidden singlet → triplet transition of HOMO/HOMO−1 → LUMO/LUMO+1 with ^{3}MLCT/^{3}ILCT characters evidenced by TD-DFT calculations, as

Table 2
Calculated absorption of **1** and **2** in CH_2Cl_2 media at TDDFT(PBE1PBE) level, together with experimental values.

Complex	Excited state	Transition	Configuration coefficient[a]	E(eV)/(nm)	f[b]	Assign[c]	Exptl (eV)/(nm)
1	$S_0 \rightarrow S_1$	H → L	0.687(100%)	3.46/358	0.062	^{1}MLCT/^{1}LLCT/^{1}ILCT	3.23/384[d]
	$S_0 \rightarrow S_5$	H−1 → L+1	0.675(94.0%)	3.93/316	0.145	^{1}MLCT/^{1}ILCT	3.67/338[d]
	$S_0 \rightarrow S_{12}$	H−3 → L	0.494(57.0%)	4.46/278	0.186	^{1}ILCT	
	$S_0 \rightarrow S_{16}$	H−2 → L+2	0.651(100%)	4.73/262	0.187	^{1}ILCT	4.81/258[d]
	$S_0 \rightarrow T_1$	H−3 → L	0.424(40.1%)	2.80/443	0.000	^{3}ILCT	3.02/411[d]
		H−1 → L+3	0.482(48.9%)			^{3}MLCT/^{3}LLCT	
2	$S_0 \rightarrow S_1$	H → L	0.682(100%)	3.05/407	0.066	^{1}MLCT	3.07/404[e]
	$S_0 \rightarrow S_2$	H−1 → L	0.689(97.6%)	3.18/390	0.262	^{1}MLCT/^{1}ILCT	3.44/360[e]
	$S_0 \rightarrow S_9$	H−4 → L	0.665(94.9%)	4.06/306	0.220	^{1}MLCT/^{1}LLCT/^{1}ILCT	4.15/299[e]
	$S_0 \rightarrow T_1$	H → L	0.566(68.7%)	2.49/498	0.000	^{3}MLCT	2.37/523[e]
	$S_0 \rightarrow T_2$	H → L+1	0.487(55.1%)	2.77/448	0.000	^{3}MLCT	2.63/472[e]
	$S_0 \rightarrow T_3$	H−1 → L	0.656(92.1%)	2.77/447	0.000	^{3}MLCT/^{3}ILCT	2.63/472[e]
	$S_0 \rightarrow T_4$	H → L+2	0.516(62.0%)	3.02/411	0.000	^{3}MLCT/^{3}LLCT	2.92/425[e]

[a] Values in parentheses are the proportion of transition configuration.
[b] Oscillator strength.
[c] These transition characters were made on the basis of the major orbital contributions. Some transition containing compared orbital contributions are assigned as mixed characters. MLCT: metal-ligand-to-ligand charge transfer; LLCT: ligand-to-ligand charge transfer; ILCT: intraligand charge transfer.
[d] From Ref. [20].
[e] From Ref. [19].

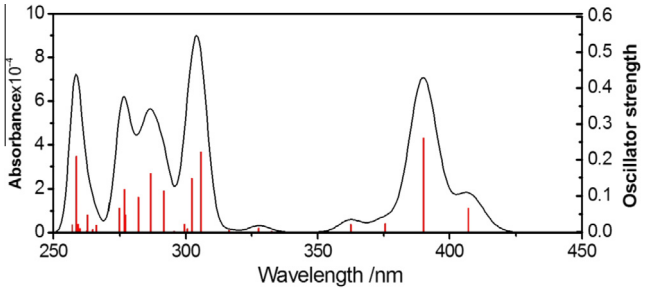

Fig. 4. Simulated absorption spectra in CH_2Cl_2 at the TDDFT (PBE1PBE)/6-31G*/LANL2DZ level for **2**. The excited states are shown as vertical bars with height equal to the oscillator strength values (red). (For interpretation of the references to color in this figure legend, the reader is referred to the web version of this article.)

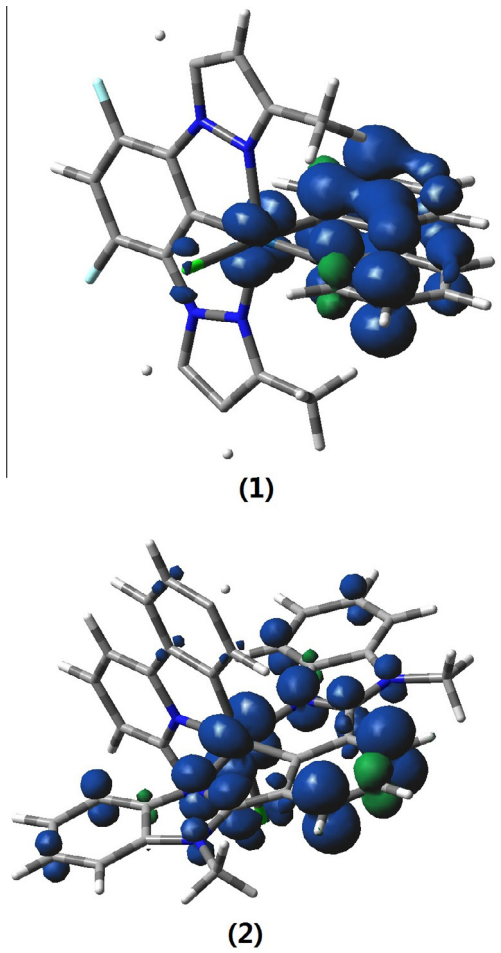

Fig. 5. Spin density distribution (isovalue = 0.004) for the lowest triplet state T1 of complexes **1** and **2**.

shown in Table 2. The triplet spin-forbidden transitions are accessible because of the large spin–orbit coupling found in the types of heavy transition metal complexes.

3.3. Triplet excited states

To further gain information on emission properties of complexes **1** and **2**, the lowest lying triplet excited states were optimized by DFT calculations and the relative structural parameters are listed in Table 1. In both cases, the lowest computed triplet excited states are all of ^{3}MLCT characters, which are confirmed by the spin density surfaces of both complexes (Fig. 5). Compared with the ground state geometries, the molecular structure discrepancy is relatively small and the Ir–N(1) and Ir–N(2) bonds for triplet are slightly shorter than for the singlet. Usually, this state is responsible for the emission according to Kasha rule [34]. However, the deactivation of the ^{3}MLCT state can occur through ^{3}MLCT → ^{3}MC pathway [35] and ^{3}MC state is a non-radiative state. Therefore, it is important to get a relationship picture of the excited states involved, which are essence for the emission process. The geometry of the lowest ^{3}MC states of both complexes were also obtained following the method presented in the literature [13,35], in which optimization is starting from the optimized ^{3}MLCT state geometry with the metal–ligand bond lengths elongated to 2.70 Å. The calculated structural parameters are also listed in Table 1. For the studied complexes, the change of the bond lengths of Ir–N(1) and Ir–N(2) is significant from the ^{3}MLCT to the ^{3}MC states. For example, the bond length of Ir–N(1) in complex **1** was elongated from 2.093 Å in ^{3}MLCT to 2.496 Å in the ^{3}MC state. As shown in Fig. 6, the spin densities of both complexes reflect the interaction along the N(1)–Ir–N(4) axis.

On the basis of the significant change of Ir–N(1) and Ir–N(4) bond lengths from the ^{3}MLCT to the ^{3}MC state, we propose that the elongation of Ir–N(1) and Ir–N(4) constitutes the reaction coordinate for the triplet excited state transformation from the ^{3}MLCT to the ^{3}MC state. The potential energy surfaces of the ^{3}MLCT were calculated as a function of Ir–N distances (Ir–N1, Ir–N4) by performing the single-point calculations. A detail calculation process was carried out as follows: starting from the lowest lying ^{3}MLCT geometry, the Ir–N(1) and Ir–N(4) distances were increased separately and independently by 0.1 Å. For each step, the Ir–N bond distance was frozen and the geometry of the molecular structure allowed to relax to a stationary point. So, the total energies of

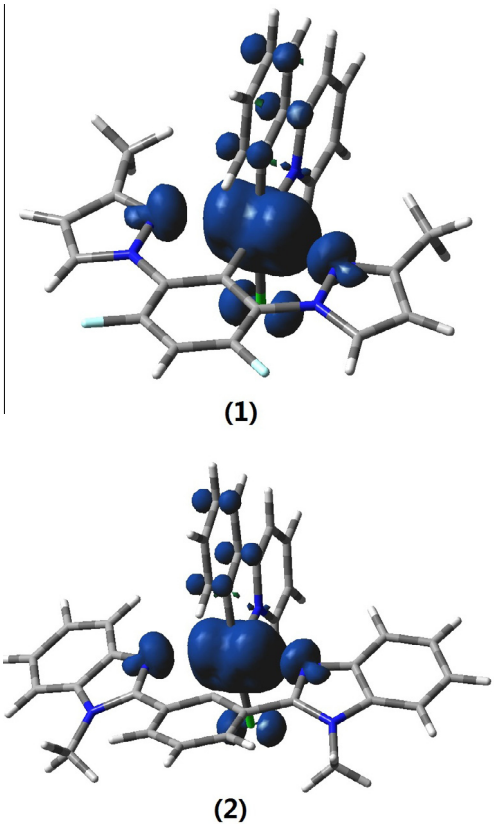

Fig. 6. Spin density distribution (isovalue = 0.004) for the triplet MC state of complexes **1** and **2**.

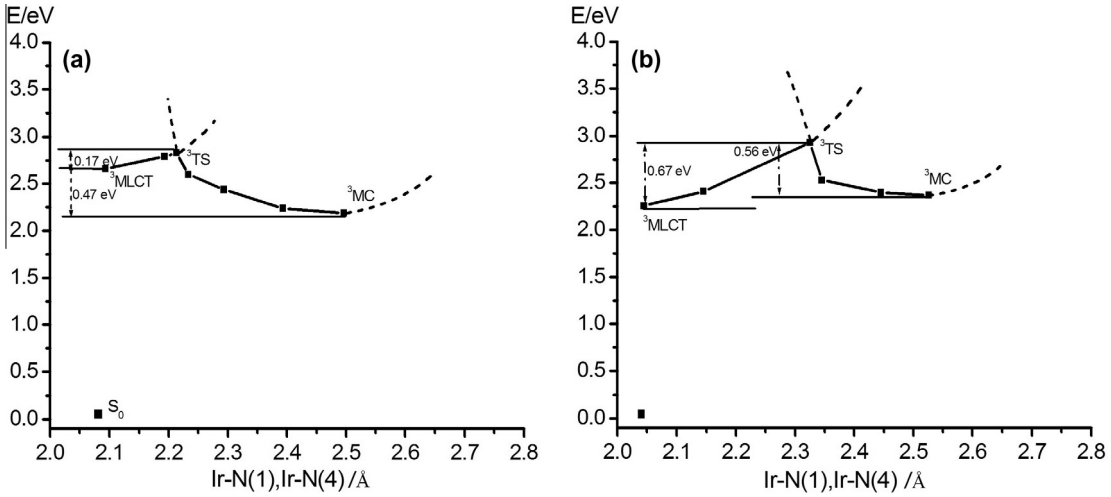

Fig. 7. Potential energy curves involving the ^{3}MLCT → ^{3}MC deactivation as a function of the bond length Ir–N(1) and Ir–N(4) for complexes **1** (a) and **2** (b).

the corresponding optimized structures were obtained. The calculated results are reported in Fig. 7.

As seen in Fig. 7, there appears to be a significant difference between the two complexes for the ^{3}MLCT → ^{3}MC relaxation pathway. For complex **1**, the ^{3}MC state is lower than the ^{3}MLCT state, indicating that the emitting species is not the most thermodynamically stable one. The energy difference between the two triplet states has substantially been reduced from 0.47 eV in complex **1** to 0.11 eV in complex **2**. Thus, the thermodynamic equilibrium between the ^{3}MLCT and ^{3}MC states is shifted towards a larger population of the ^{3}MLCT state in complex **2**, which is responsible for the good luminescence properties of complex **2**. In addition, information on the kinetics of the ^{3}MLCT → ^{3}MC deactivation requires knowing the activation barriers. The transition state (^{3}TS) between the ^{3}MLCT and the ^{3}MC state was obtained by DFT calculations. The activation barrier for the ^{3}MLCT → ^{3}MC conversion has been calculatedly estimated to be 0.17 eV for complex **1** with respect to 0.67 eV for complex **2**. Thus, from a kinetic point of view, the ^{3}MLCT → ^{3}MC conversion will be much slower in complex **2**. On the basis of these results, the differences of photophysical behaviors between complexes **1** and **2** can be rationalized. At room temperature, the available activation energy is the range of 3000–3500 cm^{-1} (about 0.37–0.43 eV) determined experimentally by the temperature dependence of the excited state decay [36,37], and it is enough energy to overcome the small activation barrier (0.17 eV) in complex **1**, leading mainly to conversion to the ^{3}MC thermodynamic state where non-radiative decay back to the ground state is efficient. Therefore, complex **1** is non-luminescent at room temperature. On the contrary, in the complex **2**, due to the higher transition activation barrier (0.67 eV), the ^{3}MC state is thermally inaccessible and the ^{3}MLCT excited state is attributed to the good luminescent efficiency.

4. Conclusions

A theoretical DFT/TD-DFT method has been used to investigate the relationship between structure and photophysical properties of two Ir complexes containing dfbpzb ligand with pyrazolyl ring and Mebib ligand with benzimidazoly ring, respectively. DFT calculation was able to predict accurately the ground state geometry of the involved complexes. In addition, calculations suggest that the substitution from dfbpzb ligand to Mebib ligand induced a significant change on the electron density of the LUMOs. The simulated absorption spectra of complexes **1** and **2** are in excellent agreement with the experimental values. A comparative study of the triplet excited states of the both complexes allowed us to rationalize the differences of their luminescence properties. The lower activation barrier calculated based on the potential energy surfaces of the ^{3}MLCT state is shown to be the principal factor for the loss of room-temperature emission for complex **1**. These preliminary studies pave the way for future investigation on the tuning of the emission properties of Ir complexes.

Acknowledgements

The authors acknowledge financial support by the National Natural Science Foundation of China (No. 20903049) and Jiangxi Science and Technology Normal University Key Laboratory of Organic-inorganic Composite Materials (Key training base). They thank the Guizhou University High Performance Computation Chemistry Laboratory (GHPCC) for help with computational studies.

References

[1] C.Y. Li, C.S. Su, H.H. Wang, P. Kumaresan, C.H. Hsu, I.T. Lee, W.C. Chang, Y.S. Tingare, T.Y. Li, C.F. Lin, W.R. Li, Dyes Pigm. 100 (2014) 57.
[2] R.D. Costa, E. Orti, H.J. Bolink, F. Monti, G. Accorsi, N. Armaroli, Angew. Chem., Int. Ed. 51 (2012) 8178.
[3] V.W.W. Yam, K.M.C. Wong, Chem. Commun. 47 (2011) 11579.
[4] S. Lamansky, P. Djurovich, D. Murphy, F. Abdel-Razzaq, H.E. Lee, C. Adachi, P.E. Burrows, S.R. Forrest, M.E. Thompson, J. Am. Chem. Soc. 123 (2001) 4304.
[5] M.A. Baldo, D.F. O'Brien, Y. You, A. Shoustikov, S. Sibley, M.E. Thompson, S.R. Forrest, Nature 395 (1998) 151.
[6] Y.M. You, W. Nam, Chem. Soc. Rev. 41 (2012) 7061.
[7] M. Wrighton, D.L. Morse, J. Am. Chem. Soc. 96 (1974) 998.
[8] S. Ladouceur, D. Fortin, E. Zysman-Colman, Inorg. Chem. 49 (2010) 5625.
[9] J.A. Simon, S.L. Curry, R.H. Schmehl, T.R. Schatz, P. Piotrowiak, X.Q. Jin, R.P. Thummel, J. Am. Chem. Soc. 119 (1997) 11012.
[10] P.S. Wagenknecht, P.C. Ford, Coord. Chem. Rev. 255 (2011) 591.
[11] M. Abrahamsson, M. Jager, R.J. Kumar, T. Osterman, P. Persson, H.C. Becker, Q. Johansson, L. Hammarstrom, J. Am. Chem. Soc. 130 (2008) 15533.
[12] C.H. Li, Y.Y. Chang, J.Y. Hung, C.Y. Lin, Y. Chi, M.W. Chung, C.L. Lin, P.T. Chou, G.H. Lee, C.H. Chang, W.C. Lin, Angew. Chem., Int. Ed. 50 (2011) 3182.
[13] T. Guillon, M. Boggio-Pasqua, F. Alary, J.L. Heully, E. Lebon, P. Sutra, A. Igau, Inorg. Chem. 49 (2010) 8862.
[14] T. Hofbeck, H. Yersin, Inorg. Chem. 49 (2010) 9290.
[15] D.W. Thompson, J.F. Wishart, B.S. Brunschwig, N. Sutin, J. Phys. Chem. A 105 (2001) 8117.
[16] K.K. Pandey, P. Patidar, Polyhedron 68 (2014) 87.
[17] R.K. Dani, M.K. Bharty, S.K. Kushawaha, O. Prakash, R.K. Singh, N.K. Singh, Polyhedron 65 (2013) 31.
[18] J.X. Wang, H.Y. Xia, W.Q. Liu, F. Zhao, Y.B. Wang, Inorg. Chim. Acta 394 (2013) 92.
[19] S. Obara, M. Itabashi, F. Okuda, S. Tamaki, Y. Tanabe, Y. Ishii, K. Nozaki, Inorg. Chem. 45 (2006) 8907.

[20] L. Yang, F. Okuda, K. Kobayshi, K. Nozaki, Y. Tanabe, Y. Ishii, Inorg. Chem. 47 (2008) 7154.
[21] E. Runge, E.K. Gross, Phys. Rev. Lett. 52 (1984) 997.
[22] S.L. Mayo, B.D. Olafson, W.A. Goddard, J. Phys. Chem. 94 (1990) 8897.
[23] P.J. Hay, W.R. Wadt, J. Chem. Phys. 82 (1985) 270.
[24] W.R. Wadt, P.J. Hay, J. Chem. Phys. 82 (1985) 284.
[25] P.C. Hariharan, J.A. Pople, Mol. Phys. 27 (1974) 209.
[26] M.S. Gordon, Chem. Phys. Lett. 76 (1980) 163.
[27] J.P. Perdew, K. Burke, M. Emzerhof, Phys. Rev. Lett. 77 (1996) 3865.
[28] J.P. Perdew, K. Burke, M. Emzerhof, Phys. Rev. Lett. 78 (1997) 1396.
[29] J. Autschbach, T. Zieglet, S.J.A. Gisbergen, E.J. Baerends, J. Chem. Phys. 116 (2002) 6930.
[30] B. Mennucci, J. Tomasi, J. Chem. Phys. 106 (1997) 5151.
[31] V. Barone, F.F. de Biani, E. Ruiz, B. Sieklucka, J. Am. Chem. Soc. 123 (2001) 10742.
[32] M. Rekhis, F. Labat, O. Ouamerali, I. Ciofini, C. Adamo, J. Phys. Chem. A 111 (2007) 13106.
[33] M.J. Frisch, G.W. Trucks, H.B. Schlegel, G.E. Scuseria, M.A. Robb, J.R. Cheeseman, J.A.Montgomery, Jr.,T. Vreven, K.N. Kudin, J.C. Burant, J.M. Millam, S.S. Iyengar, J.Tomasi, V. Barone, B. Mennucci, M. Cossi, G. Scalmani, N. Rega, G.A. Petersson, H. Nakatsuji, M. Hada, M. Ehara, K. Toyota, R. Fukuda, J. Hasegawa, M. Ishida, T. Nakajima, Y. Honda, O. Kitao, H. Nakai, M. Klene, X. Li, J.E. Knox, H.P. Hratchian, J.B. Cross, C. Adamo, J. Jaramillo, R. Gomperts, R.E. Stratmann, O. Yazyev, A.J. Austin, R. Cammi, C. Pomelli, J.W. Ochterski, P.Y. Ayala, K. Morokuma, G.A. Voth, P. Salvador, J.J. Dannenberg, V.G. Zakrzewski, S. Dapprich, A.D. Daniels, M.C. Strain, O. Farkas, D.K. Malick, A.D. Rabuck, K. Raghavachari, J.B. Foresman, J.V. Ortiz, Q. Cui, A.G. Baboul, S. Clifford, J. Cioslowski, B.B. Stefanov, G. Liu, A. Liashenko, P. Piskorz, I. Komaromi, R.L. Martin, D.J. Fox, T. Keith, M.A. Al-Laham, C.Y. Peng, A. Nanayakkara, M. Challacombe, P.M.W. Gill, B. Johnson, W. Chen, M.W. Wong, C. Gonzalez, J.A. Pople, GAUSSIAN09, Revison A 02, Gaussian Inc., Pittsburgh, PA, 2009.
[34] I.M. Dixon, F. Alary, Jean-Louis Heully, Dalton Trans. 39 (2010) 10959.
[35] M. Abrahamsson, M.J. Lundqvist, H. Wolpher, O. Johansson, L. Eriksson, J. Bergquist, T. Rasmussen, H.C. Becker, L. Hammarstrom, P.O. Norrby, B. Akermark, P. Persson, Inorg. Chem. 47 (2008) 3540.
[36] T. Sajoto, P.I. Djurovich, A.B. Tamayo, J. Oxgaard, W.A.W.A. Goddard III, M.E. Thompson, J. Am. Chem. Soc. 131 (2009) 9813.
[37] R. Czerwieniec, J.B. Yu, H. Yersin, Inorg. Chem. 50 (2011) 8293.